Off-momentum cleaning simulations and measurements at the Large Hadron Collider

Hector Garcia Morales[a,b,d], Roderik Bruce[b], Stefano Redaelli[b], Belen Salvachua[b], Joel Wretborn[b], Kyrre Ness Sjobak[b,c]

[a] *Royal Holloway University of London, Egham, United Kingdom*
[b] *CERN, Geneva, Switzerland*
[c] *Department of Physics, University of Oslo, 0316 Oslo, Norway*
[d] *currently at University of Oxford, Oxford, United Kingdom*

Abstract

The Large Hadron Collider is designed to collide proton beams with unprecedented energy in order to extend the frontiers of high-energy physics. Particles that have an energy different from the nominal one follow dispersive orbits and, if the energy offset is large enough, could be lost on the cold aperture and cause quenches of superconducting magnets. Therefore, particles with large energy offsets must be removed from the beam by the collimation system. Although the dynamics of such particles is well understood and the efficiency of the momentum cleaning is evaluated in measurements, in the past, there were not general simulations tools available for predicting the efficiency of the collimation system in scenarios where off-momentum particles are involved. In this paper we present a new set of tools to simulate off-momentum losses, the benchmarking of these tools with measurements and the evaluation of off-momentum losses in the future LHC upgrade, the HL-LHC. These new simulation tools are applied for simulating two of the main scenarios where off-momentum particles play an important role in the LHC: particles lost at the start of the energy ramp and simulations of the momentum cleaning at 6.5 TeV energy. In this study, the collimation process during dynamic changes in the machine is simulated, as opposed to previous studies in static conditions. This is the first time that this

Email address: `hector.garcia.morales@cern.ch` (Hector Garcia Morales)

sort of comparison between different simulation methods and measurements is performed. The results are used to provide a better understanding the dynamics of such particles and, finally, these tools are used to estimate the influence of off-momentum losses in the future High-Luminosity LHC.

1. Introduction

The Large Hadron Collider (LHC) [1, 2] is designed to collide 7 TeV protons and heavy ions with equivalent magnetic rigidity. The total stored energy in the proton beam reaches about 362 MJ. For the upgrade of the LHC, the high-luminosity LHC (HL-LHC) project [3], an increase of the stored energy to almost 700 MJ is foreseen. Even a small fraction of particles lost in the superconducting aperture could quench a magnet. Therefore, all beam losses need to be tightly controlled. For this purpose, a multi-stage collimation system [4, 5, 6, 7, 8] was installed in order to intercept unavoidable beam losses in a safe way. Unlike other high-energy colliders, where the main purpose of the collimation system is to reduce experimental background, the LHC requires collimation during all stages of operation to protect its elements. Out of the eight Insertion Regions (IRs) of the LHC, two are used for beam collimation, also known as beam cleaning: IR3 is devoted to momentum collimation and IR7 is devoted to betatron cleaning. In both sections a multi-stage system is installed. The multi-stage system is based on carbon-fiber-composite (CFC) primary collimators (TCP) to intercept the primary halo. Three TCPs are installed in IR7 (one per transverse plane and one skew) and one in the horizontal plane in IR3. In both cases, TCPs are followed by a series of secondary collimators (TCSGs), also made of CFC and installed downstream to absorb the secondary halo particles produced by the interaction of the primary halo with the primary collimator. Particles scattered by the TCSGs are directed to tungsten-based absorbers (TCLA). Finally, additional protection is installed around the experimental insertions where tungsten collimators (TCTs) offer extra protection to the inner triplet magnets [9, 10] and background control [11]. Identical collimation setups are implemented on both counter-rotating beams, called Beam 1 (B1) and Beam 2 (B2).

The momentum cleaning section in IR3 is designed to intercept particles with large enough momentum deviation before they reach momentum bottlenecks anywhere else around the ring like, for instance, locations with high dispersion such like arcs. For that reason, the TCP is located at a high dispersion location in the horizontal plane while keeping a relatively low β-function as can be seen in Fig. 1 for B1.

The cleaning performance of the LHC has been excellent in the first two runs up to 6.5 TeV. Before high-intensity beam is allowed in the machine, the collimation cleaning performance is qualified by inducing controlled beam losses on a safe low-intensity beam and observing the resulting loss distribution at the beam loss monitors (BLMs) around the ring [12, 13]. This is called a loss map. This essential validation is done at the different stages of the operational cycle.

In addition to the qualification of the betatron collimation cleaning inefficiency (via exciting beam particles to large transverse amplitudes), the off-momentum cleaning performance is qualified by off-momentum loss maps, where losses are induced via a shift on the RF frequency. Contrary to betatron cleaning, off-momentum cleaning in the LHC has never been simulated in detail before apart from the studies of losses from synchrotron radiation damping shown in [14].

In this paper, we consider two relevant scenarios where off-momentum losses are involved. In the first scenario, losses occurring during the first seconds at the start of the energy ramp of the beams in the LHC are simulated via a dynamic change in the reference energy of the particles. We evaluate the impact of off-momentum losses in the LHC as well as its future upgrade the HL-LHC. In the second scenario, we simulate induced off-momentum losses using an RF frequency shift as it is applied in the real machine to obtain off-momentum loss maps to validate the performance of the LHC momentum cleaning. This also represents what happens in case of RF errors which the momentum cleaning

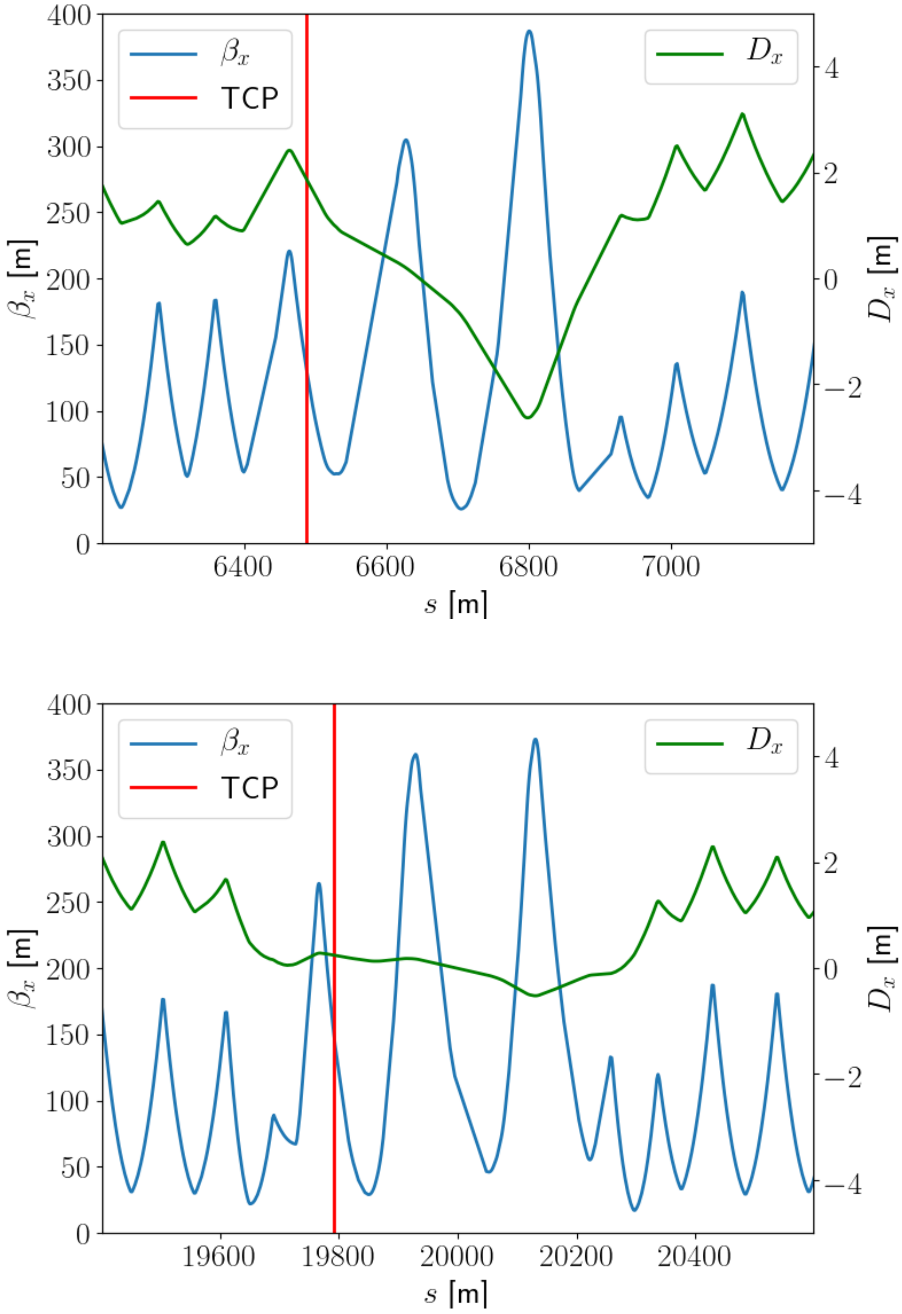

Figure 1: Optical function β_x and horizontal dispersion D_x at the momentum collimation insertion IR3 (top) and betatron collimation section IR7 (bottom) for the LHC 2017 B1 flat-top optics configuration. Similar optics are found for B2. The red line represents the location of the primary collimator in each insertion.

system protects against. In general, for the first time, we simulate the collimation process during dynamic changes in the machine, as opposed to previous studies in static conditions. These simulations provide essential information about the momentum cleaning performance not only of the present LHC but also for future configurations and upgrades.

The paper is divided in four main sections. In Sec. 2, we describe the simulations tools developed for off-momentum simulation studies and their capabilities as well as the details of the different scenarios considered later in the paper. In Sec. 3, we present studies related to the losses observed at the start of the ramp, following a detailed analysis of the recorded operational losses from the 2016 run. The off-momentum distribution at the start of the ramp was empirically fit using measured data from beam loss monitors and simulations. In Sec. 4 we present the results of applying the new set of tools to off-momentum cleaning simulations. These simulations are essential to understand the behavior and the abundance of off-momentum particles in the LHC at the different stages. In Sec. 5 simulations and projections of off-momentum related losses in the HL-LHC are presented.

2. Simulation tools

In order to reproduce with enough accuracy the dynamics of the particles circulating in the ring, realistic tracking simulation tools are required. The SixTrack code [15, 7, 16, 17] is extensively used to study the beam dynamics in the LHC. It is a multi-turn tracking code, which takes the 6D phase space into account in a symplectic manner. SixTrack performs a thin-lens element-by-element tracking through the magnetic lattice, including high-order multipoles. When a particle enters a collimator, a built-in Monte Carlo code is used to simulate the particle-matter interaction. Multiple Coulomb scattering and ionization energy loss are accounted for, as well as several point-like processes such as nuclear elastic scattering, nuclear inelastic scattering, single diffractive scattering and Rutherford scattering. A particle is considered lost either when it hits the aperture or when it interacts inelastically inside a collimator. The particle trajectories are checked for possible impacts using an aperture model with 10 cm longitudinal resolution along the 27 km circumference.

Extensive simulation campaigns are carried out for evaluating the cleaning performance of the LHC collimation system using SixTrack. In the past, betatron losses have been studied in detail and the simulation output, containing loss locations around the ring, have been compared and benchmarked to measurements [7]. Other applications of SixTrack are the simulation of LHC extraction failures [10], beam-induced experimental backgrounds [18] and recent studies on beam induced background during high-β^* run at injection [19]. For simulations of beam cleaning, the starting conditions are particle coordinates in the halo, which have already an amplitude large enough to hit a collimator. Typically, at least 6.4×10^6 halo protons are tracked for 200 turns. The simulation output contains the coordinates of all loss locations, which can be used either to directly assess the loss pattern and the cleaning efficiency, or as inputs to further simulation studies, e.g. of energy deposition.

To simulate the different scenarios involved in the study, namely losses at the start of the energy ramp and off-momentum cleaning, a turn-by-turn variation of the parameters of different machine elements is required. Using the DYNK module [20] in SixTrack, these parameters can be easily modified. The goal of the DYNK module is to make it possible to change ring element settings on a turn-by-turn basis. Many different parameters can be changed, such as magnet strengths, accelerating cavity parameters or global parameters such as the reference energy. The processes we want to reproduce would require the simulation of a large number of turns and thus a large amount of computing time. For this reason, we have considered different approaches with the aim to speed up the simulation process without losing accuracy in the prediction.

2.1. Full simulation

In this first approach, simulations reproduce the same amount of turns the procedure takes in the actual machine. Both losses at the start of the ramp and off-momentum cleaning simulations aim at reproducing the order of 10-15 seconds in the machine. This time correspond to more than 10^5 turns in the LHC. This amount of turns represents a factor 1000 the amount of turns used for betatron cleaning simulations. Machine parameters described above in each case are modified accordingly on the same timescale as in the real machine. This approach is the closest in accuracy to the actual process that takes place in the machine, but at the same time is computationally expensive and, in some cases, prohibitive. New developments in parallelization using GPUs are being implemented and could be used in the future to reduce the computation time required, which are not considered in this study.

2.2. Reduced simulation

In this second approach, we have reduced the number of simulated turns to a maximum of 10^4, a factor 10 less than the previous case. The purpose of this change is to gain computation time. In this case the reference energy or the RF frequency is still changed dynamically but over a smaller number of simulated turns, i.e. parameter variations in one simulation turn are equivalent to several real turns around the machine. All modified parameters are scaled down to the reduced number of turns. Therefore, the change per turn is larger than in the previous case. Since we are altering the physics involved, we have checked that the results are still compatible with those obtained in a more realistic scenario. Therefore, this was found to be a good compromise between simulation speed and accuracy of the results. The details on the implementation are described in the next sections.

2.3. Pencil-beam simulation

In this case, the increase in momentum offset over many turns is not simulated. Instead, the initial beam is sampled directly at the face of the primary momentum collimator in IR3, following the regular phase-space distribution matched with the machine optics. The sampling is done taking into account a realistic momentum shift in order to introduce an off-momentum orbit corresponding to an impact parameter[1] of about 1 μm at the collimator, where all particles interact in the first turn. The main advantage of this method is that it is very fast. Only a maximum of 200 turns are tracked and turns where no losses occur are avoided. The main drawback is that the dynamics as well as the losses produced while the beam is approaching the collimator cut are simplified. In addition, effects from non-linearities are highly suppressed for particles impacting on primary collimator. A dependence of the losses on the impact parameter would not be seen.

2.4. Tracking map

In addition to the full SixTrack simulations, we use for some purposes a very fast simplified tracking, using a tracking map (TM). The TM model is used mainly for scanning a large parameter space to determine which configuration should be simulated in more detail with SixTrack. The TM model is implemented as a 2+2D tracking code simulating the longitudinal phase space of the LHC. It uses a one-turn map to simulate synchrotron oscillations given by the expression [21],

$$\begin{aligned} \delta_{n+1} &= \delta_n + \frac{eV}{\beta^2 E}(\sin\phi_n - \sin\phi_s) \\ \phi_{n+1} &= \phi_n + 2\pi h \eta(\delta_{n+1})\delta_{n+1}, \end{aligned} \tag{1}$$

where h is the harmonic number, $\eta(\delta)$ is the slip factor, E is the energy of the reference particle, V is the RF voltage applied, β the reference particle speed in c units, e the electron charge, ϕ is the phase coordinate of the particle and ϕ_s is the synchronous phase that we take equal to zero for simplicity. The subscript n indicates the iteration number that corresponds to the turn number. In the transverse plane a linear one-turn map of the horizontal motion is used. For simplicity, coupling between the transverse and the longitudinal planes is

[1]The impact parameter is defined as the distance between the particle's impact and the surface of the collimator.

neglected. The interaction of particles with collimators is simplified so every time a particle reaches a the collimator jaw this particle is considered to be automatically lost. Although this is a simplified model, as it will be shown later, it represents the dynamics of the beam in the LHC required for these studies accurately enough. In this model, both IR3 and IR7 primary collimator apertures are represented.

A check of losses on the TCP is implemented through a comparison of the collimator half gap with the total particle amplitude as the sum of the betatronic and off-momentum components. Here we define the collimator half-gap by $x_{\rm cut}$, which represents the maximum aperture allowed to circulate in the LHC. From the solution of the Hill's equation, the trajectory of a particle with momentum p will cross the cut $x_{\rm cut}$ if its momentum deviation from the reference momentum p_0 is,

$$|\delta| \geq \frac{x_{\rm cut} - \sqrt{\epsilon_x \beta_x}}{|D_x|}, \tag{2}$$

where $\delta = (p - p_0)/p_0$, β_x and D_x are the horizontal β-function and dispersion function at the location of the collimator respectively and ϵ_x is the single particle emittance.

3. Off-momentum losses at the start of the energy ramp

In this section, we show measurements and simulations of the losses at the start of the energy ramp. Before showing the loss distributions around the ring, we discuss the qualitative behavior of the losses as well as the time structure.

The common operational sequence for the LHC is to inject particles at an energy of 450 GeV from the Super Proton Synchrotron (SPS). Then, the energy is increased up to its top value (so far 6.5 TeV) over about 20 minutes. Just two seconds after the start of the energy ramp, particle losses are observed at the momentum collimators in IR3. These losses, caused by unbunched beam [22], are one of the motivations for the off-momentum collimation system. A particle outside of the RF bucket follows the phase space trajectory where the ΔE compared to the reference energy decreases. In high-dispersion regions, such as

Table 1: Nominal collimator settings in beam size units used at injection energy in 2016 and 3.5 μm normalized emittance.

Collimator	IR	Half gap [σ]
TCP	3	8.0
TCSG	3	9.3
TCLA	3	12.0
TCP	7	5.7
TCSG	7	6.7
TCLA	7	10
TCT	1/5	13

the momentum collimation area, the energy offset will translate into a horizontal displacement, and the particle will eventually be lost on the machine aperture with the smallest energy cut, which is the off-momentum TCP.

In a simplified scenario where only the longitudinal motion is considered, a particle lost during the ramp can come from two different sources. Either it is outside of the bucket already at the start of the ramp or it is initially stable, but due to some process, such like a change in chromaticity [23], it jumps outside the bucket at a later stage (e.g. by the shrinkage of the bucket area when applying an accelerating phase). A consequence is that the total amount of losses is defined by the amount of unbunched beam during the injection process and the maximum ramping rate, while the rate of the losses is dependent on the rate of change of the main beam energy. In practice, the ramping function, which defines the evolution of the beam energy with time, is initially a parabola that later turns into a linear function. This particular distribution distributes the initial losses over a longer time interval than if the maximum ramp rate had been applied directly. In this section, an analysis of LHC data connected to the losses at the start of the ramp is shown and then simulations are presented in order to reproduce the observations.

Table 2: Collimator settings in beam size units, normalized to an emittance of 3.5 μm, used for the acquisition of the off-momentum loss maps (2015 LHC operational settings) during the MD with only one beam in the machine at a time. HL-LHC collimator settings have also been included for comparison.

Collimator	IR	Half gap [σ]	
		LHC	HL-LHC
TCP	3	15	15
TCSG	3	18	18
TCLA	3	20	20
TCP	7	5.5	5.7
TCSG	7	8.0	7.7
TCLA	7	14	10
TCT	1/5	13.7	10.9

In Table 1 the nominal collimator settings at injection are shown. These parameters vary along the 20 minutes-long energy ramp. However, the change during the time scale considered in this study is small enough to consider them as constant. For the simulations shown in this section, we therefore consistently use the settings in Table 1.

3.1. Time profile of losses

The analysis of the off-momentum losses at the start of the ramp was performed using 117 LHC physics fills from the 2016 run. The data set was pruned to only include fills with a total beam intensity of more than 1.8×10^{14} protons, in order to exclude fills in the commissioning and intensity ramp-up. The selected fills are representative of high-intensity fills for physics.

To understand the time evolution of losses, the BLM time profile signal from the TCP in IR3 and the horizontal TCP in IR7, for both beams, is taken. They can be compared in absolute since all four locations have comparable geometry: all collimators are in the horizontal plane, the collimators have identical design

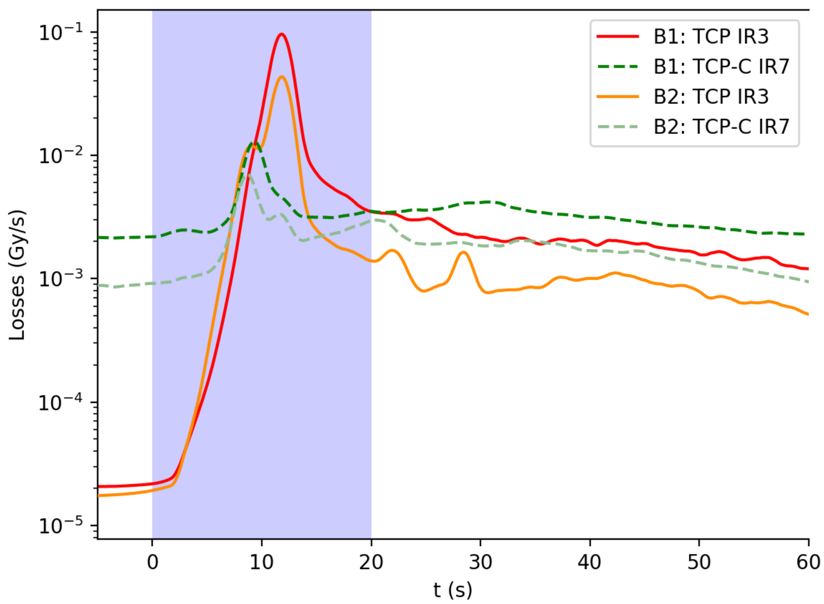

Figure 2: Measured losses of the aggregated fill as a function of the time since the start of the ramp.

and the BLM response per lost proton is expected to be very similar as the downstream placement of the BLMs in relation to the collimators is the same.

The simulations shown later are performed for the period when off-momentum losses dominate, from the start of the ramp until the crossover point. The average of the different fills is used to compare simulation results with data and to avoid possible bias in choosing a specific fill. In Fig. 2, the resulting aggregate fill is shown. As can be seen, the collimator losses are consistent between fills. In addition, the peak of losses for the aggregate fill occurs 11.8 seconds after the start of the ramp for both beams at the TCP in IR3, just a couple of seconds after the peak of losses at the location of the TCP in IR7.

Only the collimator losses are shown in Fig. 2, but an analysis has been done also for the losses on cold magnets. It is interesting to consider future cases such as the upgrade of the LHC, the HL-LHC [3], which is discussed in the last section of the paper.

3.2. Starting distribution of unbunched beam

Before simulating the losses around the ring, the initial conditions for the simulation have to be determined. They depend on the amount of unbunched beam and its distribution in energy and phase. This distribution cannot be measured easily and we therefore use a simplified simulation with the TM model to estimate it through a fit to the measured time profile of losses. The initial longitudinal phase-space coordinates for a particle at the start of the ramp will determine if it is lost and, if so, at what time. The main requirements are that the distribution is continuous and monotonically decreasing from the bucket center outwards for increasing $|\Delta E|$. Here we present an algorithm for estimating, from the LHC data and simulations, the longitudinal distribution at the start of the ramp. The majority of losses is believed to be caused by unbunched particles, but also particles initially inside the bucket but close to the separatrix can contribute.

To estimate the initial distribution, particles were placed on a grid in the longitudinal phase space, outside above (OA), outside below (OB) the bucket, and also inside (IN) the bucket close to the edge of the separatrix. The resulting probability distribution should thus also be a function of the longitudinal action of the particle J, and in the initial grid used for tracking, the density of particles was kept constant along the lines in phase space of constant J.

All particles were tracked and the time of loss on the momentum TCP was recorded. In a second step, a weight was calculated for each value of the action J using the least-square method, in order to fit the measured time profile in Fig. 2. This weighted distribution in phase space was then tracked again and the measured time profile was obtained. Further details on the method can be found in Ref. [24].

The obtained distribution $P(J)$, given for the regions OB, OA, and IN, is given by:

$$P(J) = \begin{cases} \exp\left(-20.98\frac{J}{J_{\max}} + 0.32\right) & \text{for OA,} \\ -1.16 \times 10^{-4} J + 7.14 \times 10^{-5} & \text{for IN,} \\ \exp\left(-13.03\left[\frac{J}{J_{\max}}\right]^{0.70} + 0.49\right) & \text{for OB,} \end{cases} \tag{3}$$

where $J_{\max}$ is the maximum available collimator aperture in action-value units, $J_{\max} = 3.2 \times 10^7$eV. The probability function $P(j)$ is valid for the action range $J \in [J_s - 7000\text{eV}, J_s + J_{\max}]$, and J_s is the action value at the separatrix. The inner bound of the distribution at $J_s - 7000$eV is somewhat arbitrary, but it is chosen to cover the full range inside the bucket where particles can get lost during the acceleration. The asymmetry of the distribution outside the separatrix above and below might be due to some mechanism that induces some energy loss, like impedance [25]. This point should be extended and understood in future studies, that go beyond the scope of this paper.

The likelihood α for a particle to start within one of the three regions was found to be

$$\alpha_{\text{oa}} = 0.32, \qquad \alpha_{\text{in}} = 0.2, \qquad \alpha_{\text{ob}} = 0.48. \tag{4}$$

In practice, for each particle to sample, the region was first sampled, and then Eq. (3) was used to sample its action value J. A uniform distribution of the phase ϕ between 0 and 2π was used. The final distribution, converted to units of energy deviation ΔE, is shown in Fig. 3. More details about the exact implementation of this methodology to extract the longitudinal beam distribution can be found in [24].

3.3. Loss distribution at start of ramp

Using the initial distribution shown in previous sub-section, we carry out detailed tracking simulations representing the first 11 seconds of the ramp. We have used more realistic SixTrack simulation while varying the machine parameters in order to reproduce the loss distribution around the ring. The DYNK module in SixTrack was extended to allow for simulation of an energy ramp,

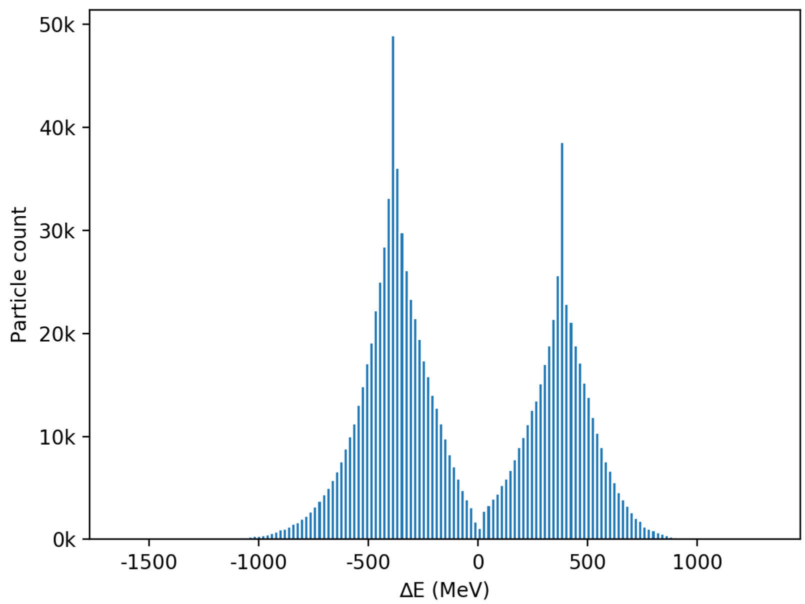

Figure 3: Input energy distribution outside of the RF bucket obtained from Eq. (3).

and it is now possible to specify a turn-by-turn value for the synchronous energy. Magnet strengths in SixTrack are calculated relative to the synchronous energy, and will increase accordingly. The approach of changing the energy of the synchronous particle is different from the conventional way to describe a ramp by an accelerating RF phase combined with a change in magnet strength. The methods, however, are equivalent, except for the fact that in DYNK the reference energy is updated only once per turn, usually when the particles start a new turn in the ring.

In Figs. 4 and 5 a comparison of measured and simulated loss maps using the full SixTrack simulation are compared. In general, we can see that simulations and measurements are in good qualitative agreement. All main loss locations are well reproduced by the simulation, with the main loss peak at the off-momentum TCP in IR3, clearly dominating over losses at the second highest peak at the betatron TCP in IR7. Since the RF trim is applied in both beams, any BLM may intercept losses from both beams, therefore, losses from both

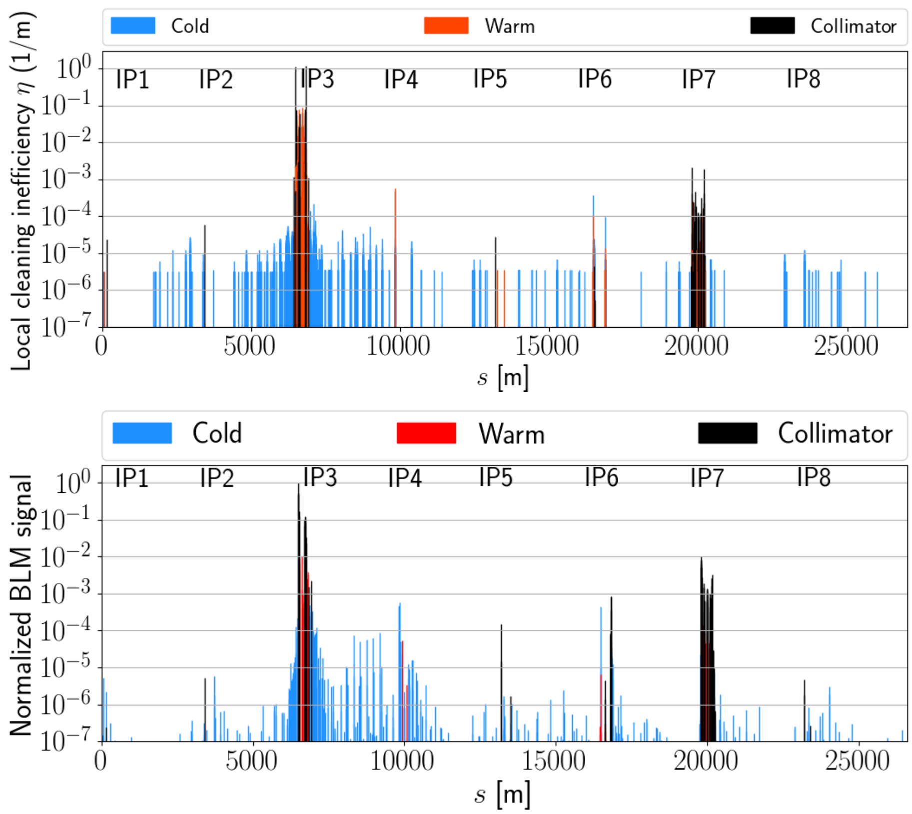

Figure 4: Comparison of simulated (top) and measured (bottom) loss map at the start of the ramp for the full LHC ring with both beams in the machine.

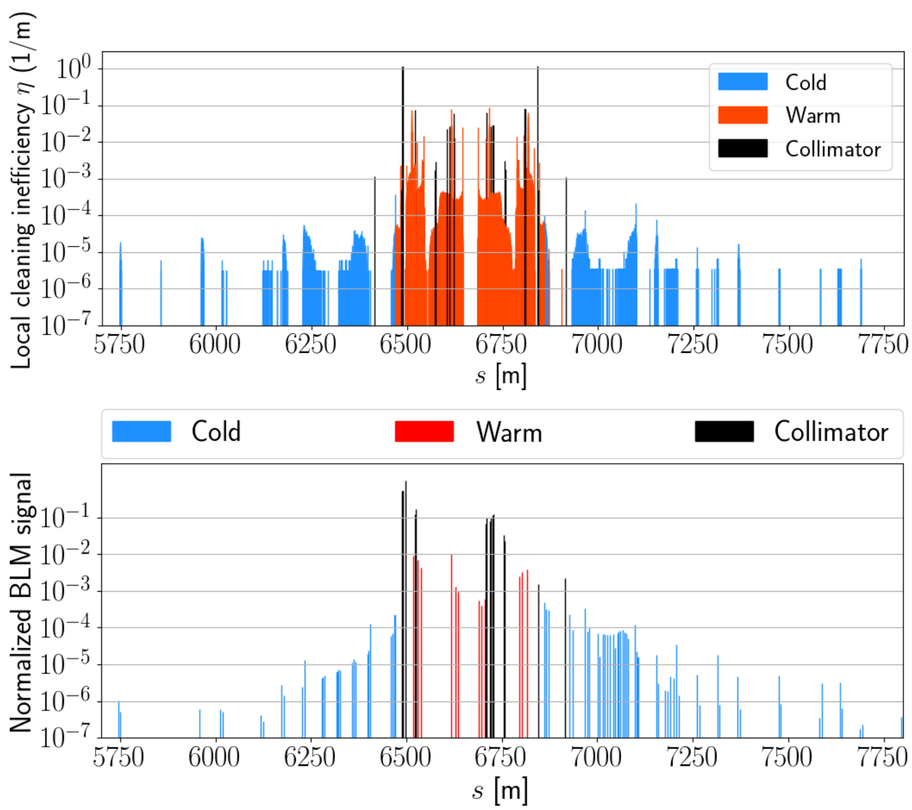

Figure 5: Comparison of simulated (top) and measured (bottom) loss map in IR3 region at the start of the ramp for the LHC with both beams in the machine.

B1 and B2 are superimposed in the measurements and are not easily distinguishable. For an easier comparison, simulations are also shown for B1 and B2 together. Additionally, all values have been normalized by the maximum BLM signal. In the measurements, the obtained losses on B1 were slightly higher, hence introducing an asymmetry between the losses at the TCPs at the right and left extremities of IR3.

When comparing the results of the simulations with the measured data we have to take into account that the measured BLM signal is accounting mainly for secondary particles generated in the interaction between primary protons and the collimator or aperture materials, while simulations only counts the primary protons lost. Experience gained in the past [7] tells us that there might be up to a factor 10 difference in the magnitude of the normalized losses between measurement and simulation. Within these uncertainties, we find a good agreement between simulations and measurements in the losses in cold sections such like in the dispersion suppressor downstream of IR3, which are 3–4 orders of magnitude lower than the primary losses on the TCP.

In Fig. 6 a comparison of the simulated loss maps using different methods described in Sec. 2 is shown in the IR3 region. The top plot is the result of the simulation using the full SixTrack simulation. The middle plot shows the same result for the simulation with the reduced number of turns. The bottom plot is obtained using the pencil beam method. The two first cases show almost identical loss patterns. In the third case, although the structure of the losses in the collimation section is almost the same preserving always the collimator hierarchy as for the previous cases, there is a significant reduction of the losses in the second cluster in the dispersion suppressor, just upstream of $s = 7100$ m from IP1 in clockwise sense.

Therefore, the two first methods are judged to be equivalent for this case. We can conclude that the accuracy of a faster simulation with reduced number of turns is not strongly affected. On the other hand, the third and simplest method, although being much faster, gives a consistent distribution of losses in the collimators but underestimates the losses in the dispersion suppressor. This is a difference that might be important in further studies for the HL-LHC.

In order to illustrate the effect of the collimator cuts and the sharing of losses between IR3 and IR7, together with the dynamics of particles in the LHC during the start of the ramp, we show in Fig. 7 the density of particles in a space consisting of normalized betatron amplitude and energy offset. This is similar to the observations found in [26]. We show a simulated snapshot of the particle distribution after 20 s. As the ramp starts, particles outside of the bucket lose energy and drift towards the left, while performing both horizontal betatron (up-down) and synchrotron oscillations (left-right). When a particle hits a collimator, its coordinates are frozen at the turn of impact. The left-most particles in the plot have impacted the lower IR3 TCP jaw, while the particles in the centre are still stable inside the RF-bucket. The few particles in between have been lost from the RF-bucket, but have not yet reached the collimators.

The cuts of the TCPs in IR7 and IR3 in this space are also shown in Fig. 7 as colored areas. For zero energy deviation, they cut the beam at their respective setting in betatron σ (5.7σ in IR7 and 8σ in IR3). At zero betatron amplitude, the dispersion function was used to determine the energy cut. Using linear optics, the space would be cut by straight lines between these points. However, we have used MAD-X [27] instead to determine the chromatic optics for a range of different energies. This causes the cuts introduced by the collimators to bend slightly and introduces a small asymmetry between positive and negative energy offsets. Since all particles perform betatron oscillations with a much faster frequency than the synchrotron motion, we have also included the mirrored cuts of both collimators (dashed lines). No particle can be outside of either of these lines, since they otherwise would be lost almost immediately when their amplitude changes sign. The allowed space for particle motion is thus constrained to be inside all physical and mirrored collimator cuts. If an unbunched particle close to the limit of the RF bucket performs betatron oscillations, moving up and down in Fig. 7, it will hit the IR7 TCP if the amplitude is large enough. If, on the other hand, it stays within the cut of this collimator, and starts moving to the left when its energy decreases during the ramp, it could hit either the

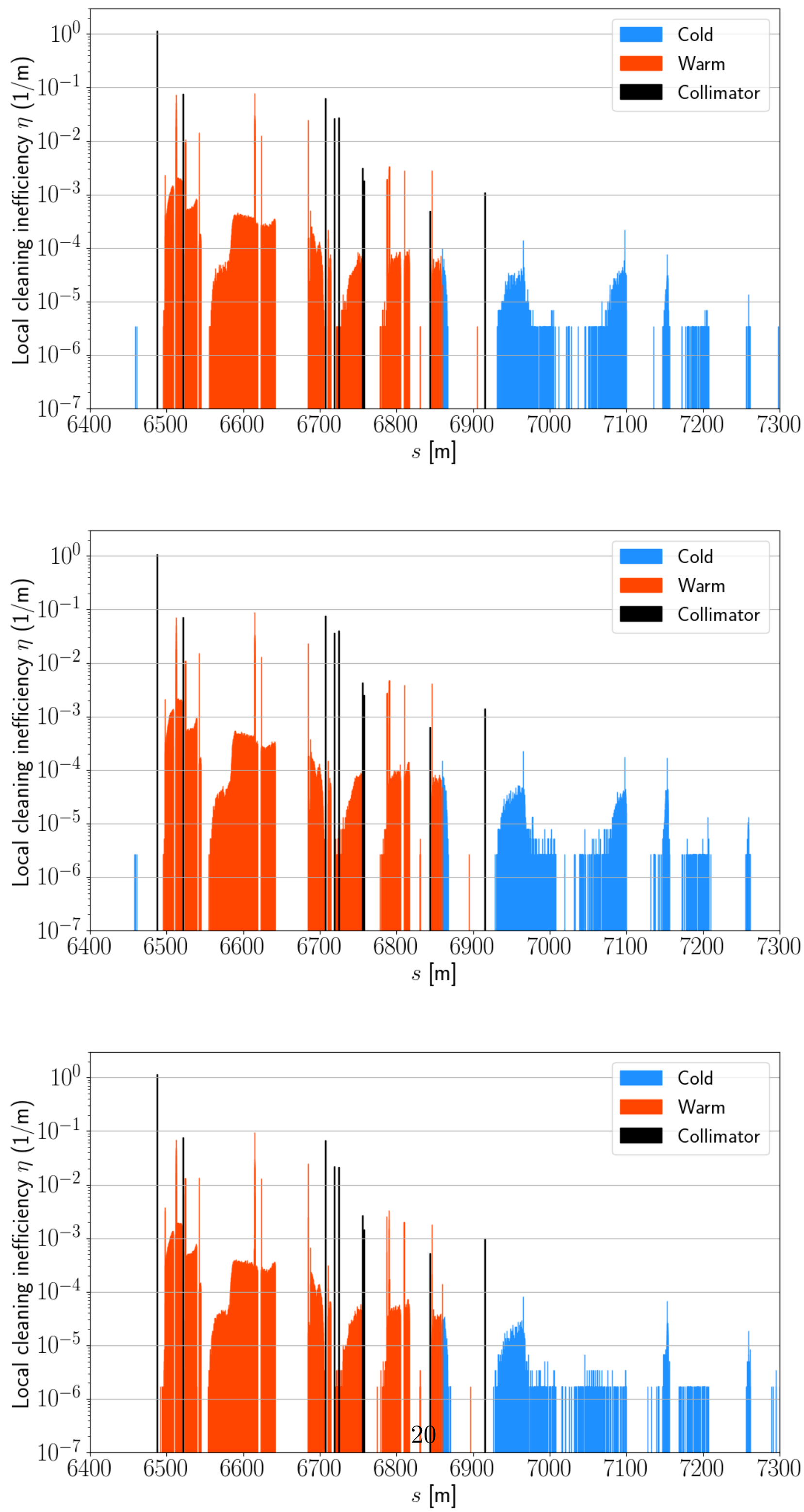

Figure 6: Simulated loss map at the start of the ramp for B1 compared for the different simulation techniques: SixTrack full (top), SixTrack reduced (middle) and using the pencil beam configuration (bottom).

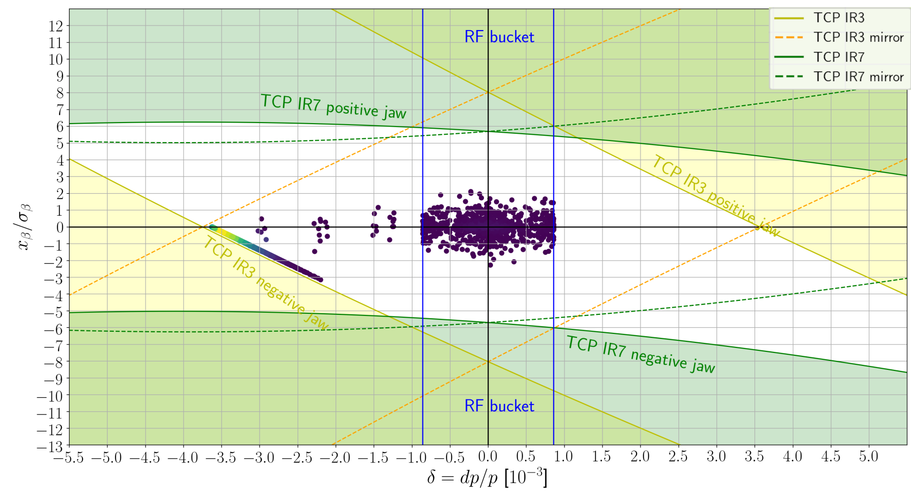

Figure 7: Two-dimensional scatter plot over particle positions after a 20 s simulation with the simplified model on top of the collimator cuts. The color of the point represents the amount of particles at the location, where a lighter colors means higher density.

IR7 or the IR3 TCP, depending on its betatron amplitude. Protons on the tails of the distribution with betatron amplitudes just inside the IR7 cut would be lost on the IR7 TCP before moving away significantly from the bucket, while protons with smaller betatron amplitudes stay longer. After a crossover point around $\delta = -10^{-3}$ the IR3 TCP takes over as limitation. Protons with the smallest betatron amplitudes will travel the longest to the left before they are lost, and it is seen that the highest density at the IR3 collimator cut is found close to a zero betatron amplitude.

4. Flat-Top off-momentum simulations

In this section we study off-momentum losses at top energy. In operation, such losses could be caused by a number of different processes, e.g. RF failures or unbunched beam losing energy through synchrotron radiation. During the off-momentum loss maps needed to qualify the collimation performance, all such losses are represented by generic off-momentum losses caused by an RF frequency shift. These loss maps have a very well defined loss source and the background noise very low, which makes them ideal for simulation benchmarks. Therefore, in the following, we show simulations of these loss maps.

4.1. Simplified RF frequency shift model

In the LHC, a dynamic change in the RF frequency is applied to introduce an off-momentum orbit to the whole beam, thus approaching it to the TCP in IR3. The applied RF frequency shift, typically introduced over about 10–15 s and reaching about -500 Hz at the end, induces a phase shift in the RF voltage seen by the synchronous particle. Then, the reference particle is not synchronous any longer for the new RF settings, creating an oscillation around the new RF bucket. If the frequency shift is applied adiabatically, i.e. with a much larger period than the period of the synchrotron oscillation ($\Omega_s = 0.0059$), the variation in the longitudinal phase space from one turn to the next is small enough to keep the entire beam captured inside the RF bucket. In this way, the full distribution is displaced towards the collimator cut. When the beam is intercepted by the collimator, losses are observed around the LHC ring using the BLMs, allowing to evaluate the efficiency of the momentum collimation system.

The RF frequency trim can be modeled adding a constant term $\Delta\varphi$ to the mapping of Eq. (1),

$$\begin{aligned} \delta_{n+1} &= \delta_n + \frac{eV}{\beta^2 E}(\sin\phi_n - \sin\phi_s) \\ \phi_{n+1} &= \phi_n + \Delta\varphi + 2\pi h\eta\delta_{n+1}, \end{aligned} \tag{5}$$

where the new term $\Delta\varphi$ represents a phase shift and is a function of the turn number (or a function of time) that represents the adiabatic change of the phase. As can be seen, the extra term shifts the reference particle and the bucket towards higher or lower values of δ. In operations, for simplicity, a linear frequency shift is applied to generate the off-momentum loss maps.

We calculate the shift in RF phase $\Delta\varphi$ as

$$\Delta\varphi(t) = \int_0^t \Delta\omega(t')dt', \tag{6}$$

where $\Delta\omega$ is the change of the RF frequency. Assuming a linear frequency change

$$\Delta\omega(t) = at, \tag{7}$$

we obtain finally

$$\Delta\varphi(t) = \frac{1}{2}at^2. \tag{8}$$

The adiabatic phase shift thus needs to be modeled as a quadratic function of time to represent a linear shift in the frequency. The coefficient of the quadratic term is given by the maximum frequency shift $\Delta\omega_{\mathrm{max}}$ and the number of turns N_{turns} during which the shift is applied,

$$a = \frac{\Delta\omega_{\mathrm{max}}}{N_{\mathrm{turns}}T_{\mathrm{rev}}}, \tag{9}$$

with T_{rev} being the revolution time.

Inserting this value of a in Eq. (8), and changing the independent variable to the number of turns n, we obtain finally

$$\Delta\varphi_{\mathrm{cav}}(n) = \frac{\Delta\omega T_{\mathrm{rev}}}{2N_{\mathrm{turns}}}n^2. \tag{10}$$

Eq. (10) is taken in tracking simulations using SixTrack to change dynamically the RF cavity phase. In the next sections we apply this formalism to set up a realistic simulation model.

To test this description of the dynamics of the particles during the frequency shift, a simplified analytical model has been created where the longitudinal motion of the beam is computed using Eq. (5). The motion of the particles in the phase space is studied to get an approximate idea of the key observations involved. We tested the simple model for a total RF frequency shift of $\Delta f_{\mathrm{RF}} = 2\pi\Delta\omega_{\mathrm{RF}} = -500\,\mathrm{Hz}$. This corresponds to a maximum phase shift of about $\Delta\varphi_{\mathrm{max}} \approx 0.28\,\mathrm{rad}$. The maximum momentum deviation for the maximum shift is about $|\delta| = 3.8 \times 10^{-3}$. This simple model shows that, for the nominal collimator half-gap of the primary momentum collimator at 15σ (Table 2), we are able to predict that the core of the bunch will cross the collimator cut when the $\Delta f_{\mathrm{RF}} \sim 300$ Hz. This corresponds to a momentum deviation of

$|\delta| = 1.6 \times 10^{-3}$. Therefore, it is expected that the full beam will be intercepted by the IR3 TCP for frequency shifts significantly beyond that.

4.2. Cleaning simulation setup

The model described above has been implemented using the more realistic tracking in SixTrack.

To implement the RF frequency shift, we have used the DYNK module, also described previously, which allows to dynamically change some parameters of the simulation. For our purposes, the goal is to dynamically change the cavity phase turn-by-turn accordingly to Eq. (10). Then, particles are tracked around the ring while the phase shift is carried out and the hits in the aperture and particles absorbed by the collimators are recorded. From this, we can reconstruct the off-momentum loss maps.

In the result of the simulation of an off-momentum loss map, the main losses occur in the momentum collimation section (IR3). Nevertheless, as it is also observed during the loss maps acquisition, one can observe some losses in the betatron cleaning section (IR7). These losses are due to the fact that, on one hand, for low frequency shifts the primary bottleneck is still the betatron primary collimator. On the other hand, there is also leakage of secondary and tertiary halo particles out of IR3 that is likely to impact in IR7. In Fig. 8, the losses at the primary betatron collimator in IR7 and the primary momentum collimator in IR3 as a function of the frequency shift after SixTrack simulations are shown. One can see that, beyond 200 Hz, the momentum collimator in IR3 becomes the primary collimator intercepting most of the lost particles. As predicted from the simple model described previously, the full beam distribution is scraped completely by the collimation system when the frequency shift is above 300 Hz.

Having the evolution of losses during the frequency shift at the different collimators is important. During the off-momentum loss map acquisition in the machine, the losses around the ring are integrated for a short time (usually 1.3 seconds) when losses at the momentum collimator are around their maximum

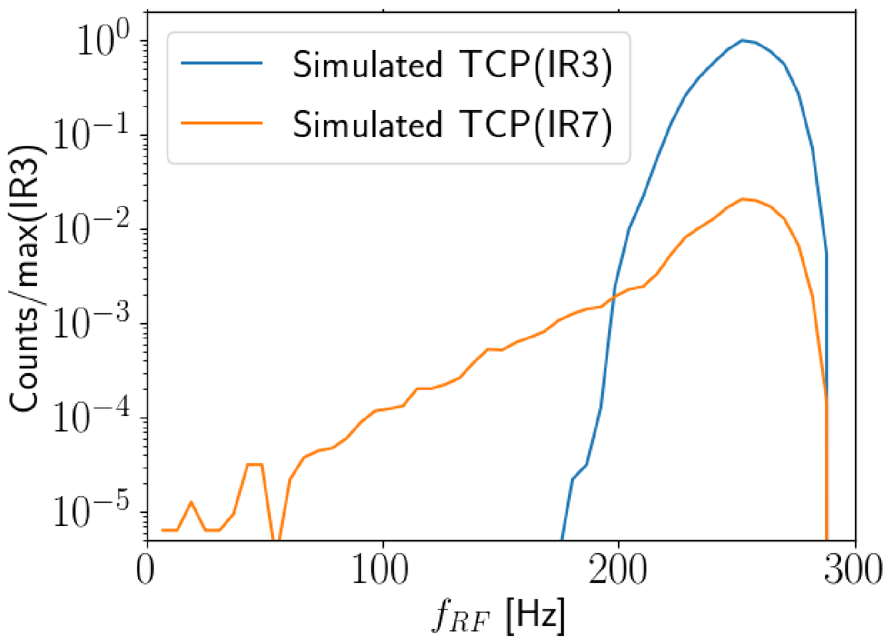

Figure 8: Evolution of the losses at the primary betatron collimator in IR7 and the primary momentum collimator in IR3 as a function of the frequency shift f_{RF} of -500 Hz during 10^4 turns. Losses are normalized to the peak losses in IR3.

value. Therefore, in order to compare more accurately to the observations, simulated losses spanning the equivalent of 1.3 seconds are integrated around the time intervals with higher losses in the momentum primary collimator. Taking into account that the full trim of -500 Hz is carried out in about 15 seconds, an integration time of 1.3 sec would correspond to a change in frequency of about 43 Hz. Therefore, the resulting loss map is obtained taking into account integrated losses from the frequency corresponding to the time of the largest loss in IR3, integrated around it over a time interval during which the RF frequency shift by 43 Hz.

During the actual off-momentum loss map acquisition, protons in the LHC perform more than 1.5×10^5 turns. In order to reduce the simulation time, simulations with a smaller number of turns were performed, as discussed in Sec. 2. The risk of decreasing the number of turns is that if the RF frequency shift between two consecutive turns is large enough, further particles that are captured might eventually be lost from the bucket. To investigate this effect on the final loss pattern around the ring, different simulations using different number of turns have been performed.

The total number of lost particles on the aperture or collimators at the end of the simulation as a function of the number of turns was simulated. A clear reduction of the number of lost particles is observed when the frequency shift is performed during a small number of turns. For above 10^4 turns, more than 99% of the particles are always within the RF bucket and are lost either in the magnet aperture or the collimators.

4.3. Results

During Run 1 and Run 2, several measurements of the off-momentum loss maps using the RF trim were taken during machine commissioning, always with both beams present in the machine. In order to disentangle the contributions of losses coming from both beams, specific machine development sessions with only one beam in the machine were carried out and off-momentum loss maps for each beam were taken [28]. These results are used for benchmarking the new set of simulation tools described above. In Fig. 9 the off-momentum loss maps obtained with only one beam in the machine and with the collimation settings in Table 2 are shown for B1 (top) and B2 (bottom) at flat top energy. For both cases, a negative frequency shift was applied during approximately 15 seconds with a maximum frequency shift of -500 Hz. Losses generated by the frequency shift are usually above the safety limits set for the BLM readings and the beam was dumped when the frequency shift was around 250–300 Hz, before reaching the maximum frequency shift. Simulations show that the beam is, in any case, fully scraped by the collimator at a frequency shift slightly below 300 Hz. This is in line with the predictions from simulations presented above.

In Fig. 10 and Fig. 11 the measured loss maps (top plots) are compared to the simulated loss maps for B1 using the two methods explained in previous sections (middle and bottom plots). In the reduced simulation with 10^4 turns, a -500 Hz total frequency shift was applied. In the pencil-beam method, the beam was sampled directly at the TCP in IR3 using a reference energy of 6513 GeV, which represents an energy deviation of $\delta = 0.2\%$. This value was found to represent an impact parameter at the TCP of about 1 μm. One can see that one difference between the results of the two simulation methods is in the ratio of losses between IR3 and IR7 primary collimators. When using the reduced simulation, the difference is about one order of magnitude, while it is slightly smaller with the pencil beam. When we look at the details of the loss map in IR3 (Fig. 11) we can see that the differences are almost negligible. Therefore, these two methods can be considered equivalent as far as local IR3 losses are concerned.

As for the comparison with BLMs at the start of the ramp, it should be pointed out that some differences are expected, possibly up to around a factor 10 [7]. This is because the simulation accounts only for the number of protons lost locally, while the BLMs are sensitive to the secondary showers resulting from the impacts. On the other hand, longitudinal locations where losses occur should be well comparable.

Furthermore, we note that the BLM response is slightly different for different

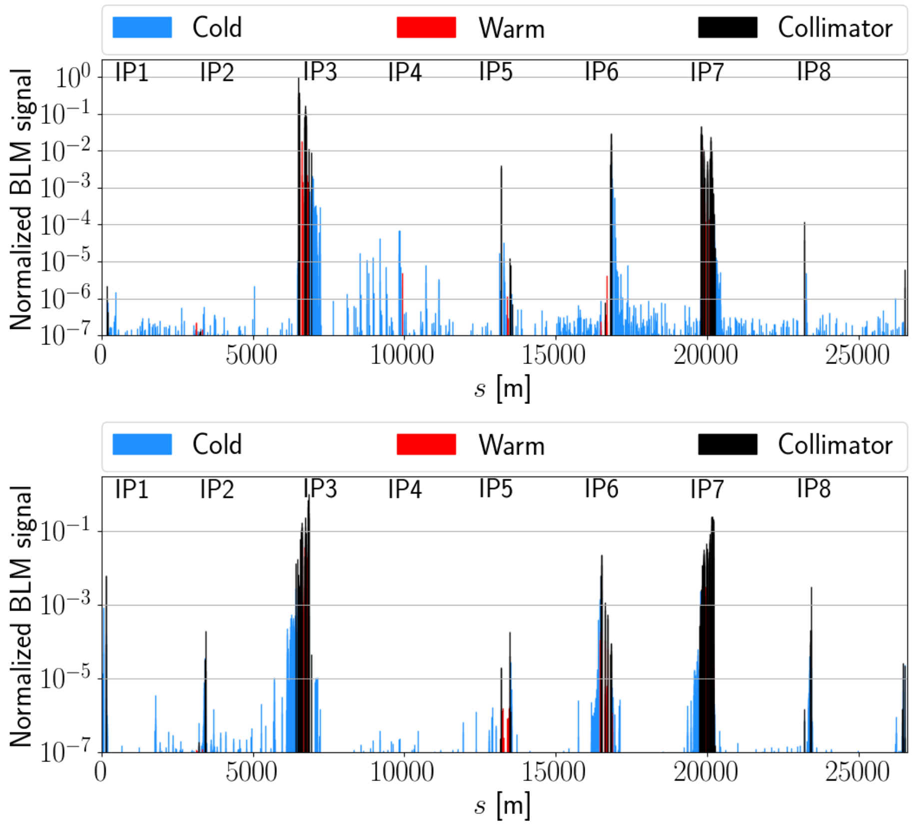

Figure 9: Measured off-momentum loss maps at 6.5 TeV for B1 (top) and B2 (bottom) for a frequency shift of -500 Hz, obtained with only one beam in the machine and with the collimation settings in the Table 2.

BLMs. Therefore, we can only compare quantitatively the magnitude of the signal between those BLMs which we know have a similar response. This is the case of, e.g., the BLMs installed close to the TCPs in IR3 and IR7, although even for those BLMs, differences may occur due to differences in impact parameter distribution. One can see that the ratio of losses measured at these TCPs is in good agreement with simulations, in particular when we consider the simulation scenario with reduced number of turns. In both cases we observe a ratio of about one order of magnitude.

Concerning loss locations, all plots show a similar distribution of losses. In particular, in the regions were collimators are located, the measurements and simulations agree quite well and the key loss locations reproduced. Losses produced in the aperture are well represented in particular in IR4, were we can observe losses in all the cases following a similar pattern. On the other hand, betatron losses do typically not impact in IR4. In terms of loss magnitudes, we observe some discrepancy in IR6 where measured losses at the collimators are significantly higher than in simulations. Similar discrepancies were observed in IR6 for betatron losses, and detailed energy deposition studies should be performed to quantify if they can be explained by the showering and BLM response. Nevertheless, this discrepancy does not affect the most important comparison at the cleaning insertions, where the comparison is more reliable. From these results, we can conclude that the simulation procedure describes the observations and, therefore, can be used for future analysis of other configurations and upgrades.

5. HL-LHC

The new set of tools presented in previous sections can be used to evaluate the impact of off-momentum losses in the future upgrade of the LHC, the HL-LHC project [3]. In this section we present simulations of the two scenarios described above using HL-LHC optics v1.3. This is an important input for the future LHC upgrade since it will provide essential information for the understanding of the cleaning performance of the collimation system after the intensity increase and the optics changes in the high luminosity interaction points.

5.1. Losses at the start of the ramp

A bunch intensity increase by a factor 2 [3] is foreseen for the HL-LHC. Assuming the same capture efficiency, this would double the energy deposited in downstream magnets at the start of the ramp with respect to the LHC. In this case we also assume that the beam distribution in the longitudinal plane is not significantly affected for the purpose of these studies.

Simulations of the start of the ramp for the HL-LHC injection optics have been performed, using the same setup as in Sec. 3. We assumed that the energy ramp follows the same time function as the LHC ramp at the start. Since the change from the LHC injection optics to the HL-LHC injection optics is minor, it is expected that the results in both cases are comparable. This is confirmed by simulations as one can see in Fig. 12, where the loss map obtained is shown for B1. This loss map can be compared to the one obtained for the LHC and shown in Fig. 4 and Fig. 5. No significant difference is appreciated.

In addition to the simulations performed, measured peak losses at the start of the ramp have been analyzed for several fills in 2017 run and compared to the beam dump thresholds. The fills with a full machine, i.e. with around 3×10^{14} protons per beam, were selected. The analysis of losses reveals that the peak losses in cold magnets downstream of momentum cleaning section are of the order of 4×10^{-5} Gy/s while the dump threshold is about 1×10^{-2} Gy/s, i.e. more than two orders of magnitude higher. Only in some cases 1% of the beam dump threshold was reached for integration times (also known as running sums) of 1.3 seconds. Losses for larger and smaller running sums were also checked and in all cases the same trend was found. In the rest of the fills the value was below that number. Therefore, extrapolating to HL-LHC beam intensities, expected to be twice the LHC beam intensity, the expected maximum will be about 2% of the beam dump threshold, provided that the cleaning efficiency in IR3 does not change significantly. As seen by comparing Figs. 12 and 4, this is indeed the case. This analysis confirms that the losses at the start of the ramp will not impose any limitation for the future LHC upgrade unless unexpected issues occur. In addition, recent plans to reduce the RF voltage to 5 MV to cope with limitations during transients may have some impact on the amount of losses produced at the start of the ramp in the HL-LHC. However, the impact on losses is expected to be small.

Table 3: Peak losses during the start of the ramp using BLM signal with a running sum of 1.3 seconds.

Fill	Peak Losses	HL losses	Threshold	Dump Ratio
	$[10^{-4}$ Gy/s]		[Gy/s]	[%]
5433	1.27	2.6	0.10	0.13
6643	275	550	2.68	1
6646	216	432	2.68	0.8
7124	4.65	9.3	0.1	0.04

5.2. Off-momentum loss map simulations

Off-momentum cleaning simulations have been performed at 7 TeV for the HL-LHC optics v1.3 and 15 cm collision optics. The simulation settings used are those shown in Table 2. The RF voltage is set to the nominal value of 8 MV, and an RF frequency shift of ±500 Hz is simulated for 10^4 turns and losses around the ring are recorded. In Fig. 13 the evolution of losses in the primary collimators in IR3 and IR7 as a function of the negative frequency trim is shown. If we compare this result with the result obtained for the LHC shown in Fig. 8, although losses in IR7 seem to start a bit later probably due to the more relaxed collimator setting (for frequencies above 100 Hz), losses in IR3 overtake losses in IR7 around the same frequency shift (200 Hz). In addition, the beam is fully scraped just after 250 Hz, earlier than the 300 Hz observed for the LHC. This is due to the fact that for HL-LHC we used an RF voltage of 8 MV while for the LHC 12 MV was used instead. A modification of the RF voltage modifies the topology of the longitudinal phase space and thus the properties, such as the bunch length and dynamics of the bunch. In this case, the voltage reduction is translated into a smaller bucket height and thus the beam is compressed in a smaller area (considering the same frequency shift). For that reason, the beam is scraped faster when lower voltages are used.

In Fig. 14 the simulated off-momentum loss map for B1 is shown. In general one can see that distribution of losses in the different collimators around the ring is similar to the one obtained for the LHC. An interesting result is that no losses leaking from IR7 are observed. This is due to the addition of the new collimators in the dispersion section (TCLDs). Furthermore, higher losses in cold aperture are found in IR4 compared to the LHC. In IR3 (Fig. 14 bottom), the distribution of losses is similar to the distribution observed for the LHC although both the peak losses and integrated loss in the two clusters of the dispersion suppressor are slightly higher in the HL-LHC. This level of losses should be within the tolerances margins. A more detailed study, beyond the scope of this paper, of the energy deposited in these magnets should be carried out to quantify the amount of losses in IR3 that would cause a quench.

Nevertheless, we conclude that the current design of the momentum cleaning insertion of the HL-LHC is efficient enough to remove off-momentum particles without imposing any hazard to the machine.

6. Conclusions

A new set of simulation tools based on a realistic particle tracking code (SixTrack) has been developed to study different scenarios where losses of off-momentum particles are involved after a benchmarking with measurements. Two main scenarios have been considered: losses produced at the start of the ramp and off-momentum loss maps at 6.5 TeV using an RF frequency shift. These cases are relevant for studying potential limitations for LHC and HL-LHC and for detailed benchmark to measured data. This is a new methodology that is very useful in particular when the actual impact parameter is unknown. On top of that, we simulate the collimation process during dynamic changes in the machine, as opposed to previous studies in static conditions.

More than one hundred fills were used to analyze the loss pattern observed in the LHC during the start of the ramp. The analysis reveal that the behavior from fill to fill is very reproducible. It was also shown that the most important contribution of off-momentum losses occur within the first 12 seconds after the start of the ramp. Simulations show a very good agreement with the measurements. From the data extracted, the beam distribution was fitted and used in tracking simulations. The loss maps obtained from these simulations are in good agreement with the measurements and could be used for predicting losses for future LHC configurations. These tools have allowed to fit the longitudinal distribution on the ramp losses. This provided an understanding of the number of particles populating the RF bucket close to the separatrix and the fitted semi-analytical model can be used in the future for different machine configurations.

In the second scenario, we have simulated the cleaning of off-momentum particles in the LHC at 6.5 TeV during the measurement of off-momentum loss maps. We can now evaluate the efficiency of the momentum cleaning of the LHC in any possible configuration. These tools also provide essential information about the population of the off-momentum halo and for the optimization of the momentum cleaning insertion.

In the two scenarios considered above, we have demonstrated that it is not needed to simulate the full process taking into account the total amount of turns. A significant reduction of the number of turns in the simulation, to about 10^4 turns, is enough to reproduce with enough accuracy what is observed in the real machine. Even further, a simple simulation method using a pencil beam sampled directly at the collimator surface has been proven to be almost as accurate in the case of reproducing off-momentum cleaning losses, although losses at the start of the ramp in the dispersion suppressor are slightly underestimated.

Losses along the ring were also computed finding a qualitative agreement with measured loss maps for both the LHC but also for its future upgrade, the HL-LHC. Losses for the two scenarios considered have been evaluated for HL-LHC. Slightly higher losses were found with respect to the LHC but always below tolerances. It was also found that, due to the change in the RF voltage, the bunch is fully scraped at lower frequencies with respect to the LHC. This will need to be further investigated in case the RF voltage is further reduced to 5 MV. In general, we have seen that off-momentum losses are not expected to be a limiting factor for neither the Run 3 of the LHC nor for the HL-LHC as injection time is kept at similar levels as in Run II.

This new set of tools will be also useful to optimize the collimation system in future larger machines, such as the Future Circular Collider [29, 30].

Acknowledgements

The authors are really grateful to Gianluigi Arduini, Massimo Giovannozzi and Rogelio Tomas for their comments and suggestions, which significantly increased the quality of the manuscript.

References

[1] O.S.Bruning, P. Collier, P. Lebrun, S. Myers, R. Ostojic, J. Poole, P. Proudlock, CERN report No. CERN-2004-003-V1 (2004).

[2] L. Evans, P. Bryant, JINST, 3, S08001 (2008).

[3] G. Apollinari, et al., High-luminosity large hadron collider (hl-lhc) : Technical design report v. 0.1, CERN-2017-007-M (2017).

[4] R. Assmann, Collimators and beam absorbers for cleaning and machine protection, Proceedings of the LHC Project Workshop - Chamonix XIV, Chamonix, France (2005) 261.

[5] R. Assmann, et al., The final collimation system for the lhc, Proceedings of the European Particle Accelerator Conference 2006, Edinburgh, Scotland (2006) 986.

[6] J. B. Jeanneret, Phys. Rev. ST Accel. Beams 1, 081001 (1998).

[7] R. R. Bruce, R. W. Assmann, V. Boccone, C. Bracco, M. Brugger, M. Cauchi, F. Cerutti, D. Deboy, A. Ferrari, L. Lari, A. Marsili, A. Mereghetti, D. Mirarchi, E. Quaranta, S. Redaelli, G. Robert-Demolaize, A. Rossi, B. Salvachua, E. Skordis, C. Tambasco, G. Valentino, T. Weiler, V. Vlachoudis, D. Wollmann, Simulations and measurements of beam loss patterns at the CERN large hadron collider, Phys. Rev. ST Accel. Beams 17 (2014) 081004. doi:10.1103/PhysRevSTAB.17.081004.
URL https://link.aps.org/doi/10.1103/PhysRevSTAB.17.081004

[8] G. Valentino, G. Baud, R. Bruce, M. Gasior, A. Mereghetti, D. Mirarchi, J. Olexa, S. Redaelli, S. Salvachua, A. Valloni, J. Wenninger, Final implementation, commissioning, and performance of embedded collimator beam position monitors in the large hadron collider, Phys. Rev. Accel. Beams 20 (2017) 081002. doi:10.1103/PhysRevAccelBeams.20.081002. URL `https://link.aps.org/doi/10.1103/PhysRevAccelBeams.20.081002`

[9] R. Bruce, R. W. Assmann, S. Redaelli, Calculations of safe collimator settings and β^* at the CERN Large Hadron Collider, Phys. Rev. ST Accel. Beams 18 (2015) 061001. doi:10.1103/PhysRevSTAB.18.061001. URL `http://link.aps.org/doi/10.1103/PhysRevSTAB.18.061001`

[10] R. Bruce, C. Bracco, R. D. Maria, M. Giovannozzi, A. Mereghetti, D. Mirarchi, S. Redaelli, E. Quaranta, B. Salvachua, Reaching record-low β^* at the CERN large hadron collider using a novel scheme of collimator settings and optics, Nuclear Instruments and Methods in Physics Research Section A: Accelerators, Spectrometers, Detectors and Associated Equipment 848 (2017) 19 – 30. doi:https://doi.org/10.1016/j.nima.2016.12.039. URL `http://www.sciencedirect.com/science/article/pii/S0168900216313092`

[11] R. Bruce, R. Assmann, V. Boccone, G. Bregliozzi, H. Burkhardt, F. Cerutti, A. Ferrari, M. Huhtinen, A. Lechner, Y. Levinsen, A. Mereghetti, N. Mokhov, I. Tropin, V. Vlachoudis, Sources of machine-induced background in the ATLAS and CMS detectors at the CERN Large Hadron Collider, Nucl. Instrum. Methods Phys. Res. A 729 (0) (2013) 825 – 840. doi:10.1016/j.nima.2013.08.058.

[12] E. Holzer, et al., Beam loss monitoring system for the lhc, IEEE Nucl. Sci. Symp. Conf. Rec. 2 (2005) 1052.

[13] E. Holzer, et al., Development, production and testing of 4500 beam loss

monitors, Proceedings of the European Particle Accelerator Conference 2008, Genoa, Italy (2008) 1134.

[14] E. Quaranta, R. Bruce, S. Redaelli, Sixtrack simulation of off-momentum cleaning in lhc, Proceedings of IPAC13, Shanghai, China (2013).

[15] F. Schmidt, CERN Report No. CERN/SL/94-56-AP (1994).

[16] G. Robert-Demolaize, R. Assmann, S. Redaelli, F. Schmidt, A new version of sixtrack with collimation and aperture interface, Proceedings of the Particle Accelerator Conference 2005, Knoxville (2005) 4084.

[17] S. Redaelli et al., Proceedings of the icfa mini-workshop on tracking for collimation (Jun 2018).
URL https://doi.org/10.23732/CYRCP-2018-002.1

[18] R. Bruce, M. Huhtinen, A. Manousos, F. Cerutti, L. Esposito, R. Kwee-Hinzmann, A. Lechner, A. Mereghetti, D. Mirarchi, S. Redaelli, B. Salvachua, Collimation-induced experimental background studies at the CERN Large Hadron Collider, Phys. Rev. Accel. Beams 22 (2019) 021004. doi:10.1103/PhysRevAccelBeams.22.021004.
URL https://link.aps.org/doi/10.1103/PhysRevAccelBeams.22.021004

[19] D. Mirarchi et al., Experimental evidence of reduced beam-related background on forward physics detectors using crystal collimation at the large hadron collider, Submitted to PRX (2020).

[20] K. Sjobak, et al., New features of the 2017 sixtrack release, CERN-ACC-2017-114 (2017).

[21] Chao, Alexander Wu and Tigner, Maury, Handbook of Accelerator Physics and Engineering, World Scientific, Singapore, 1999.
URL https://cds.cern.ch/record/384825

[22] J. Jeanneret, Momentum losses in LHC: the special case of rf uncaptured protons, CERN SL-Note-92-56-EA (1992).

[23] M. Schaumann et al., Tune and chromaticity control during snapback and ramp in 2015 LHC operation, IPAC conference proceedings, 2016.

[24] S. Wretborn, R. Bruce, H. G. Morales, K. Sjobak, Study of off-momentum losses at the start of the ramp in the Large Hadron Collider, CERN-ACC-NOTE-2017-0065 (2017).
URL `https://cds.cern.ch/record/2298696`

[25] T. Bohl, T. Linnecar, E. Shaposhnikova, J. Tuckmantel, Studies of the capture loss of the lhc beam in the sps, AB-Note-2004-036 MD (2004).

[26] C. Bracco, Commissioning scenarios and tests for the lhc collimation system, Ph.D thesis (2008).

[27] [link].
URL `http://cern.ch/mad/`

[28] H. Garcia Morales, R. Bruce, B. Salvachua, Off-momentum loss maps with one beam, CERN-ACC-NOTE-2016-0011 (Jan 2016).
URL `https://cds.cern.ch/record/2121307`

[29] A. Abada, et al., FCC-hh: The Hadron Collider, The European Physical Journal Special Topics 228 (4) (2019) 755–1107. doi:10.1140/epjst/e2019-900087-0.

[30] R. Bruce, A. Abramov, A. Bertarelli, M. Besana, F. Carra, F. Cerutti, A. Faus-Golfe, M. Fiascaris, G. Gobbi, A. Krainer, A. Lechner, A. Mereghetti, D. Mirarchi, J. Molson, M. Pasquali, S. Redaelli, D. Schulte, M. Serluca, E. Skordis, M. Varasteh, , Journal of Physics: Conference Series 1350 (2019) 012009. doi:10.1088/1742-6596/1350/1/012009.
URL `https://doi.org/10.1088%2F1742-6596%2F1350%2F1%2F012009`

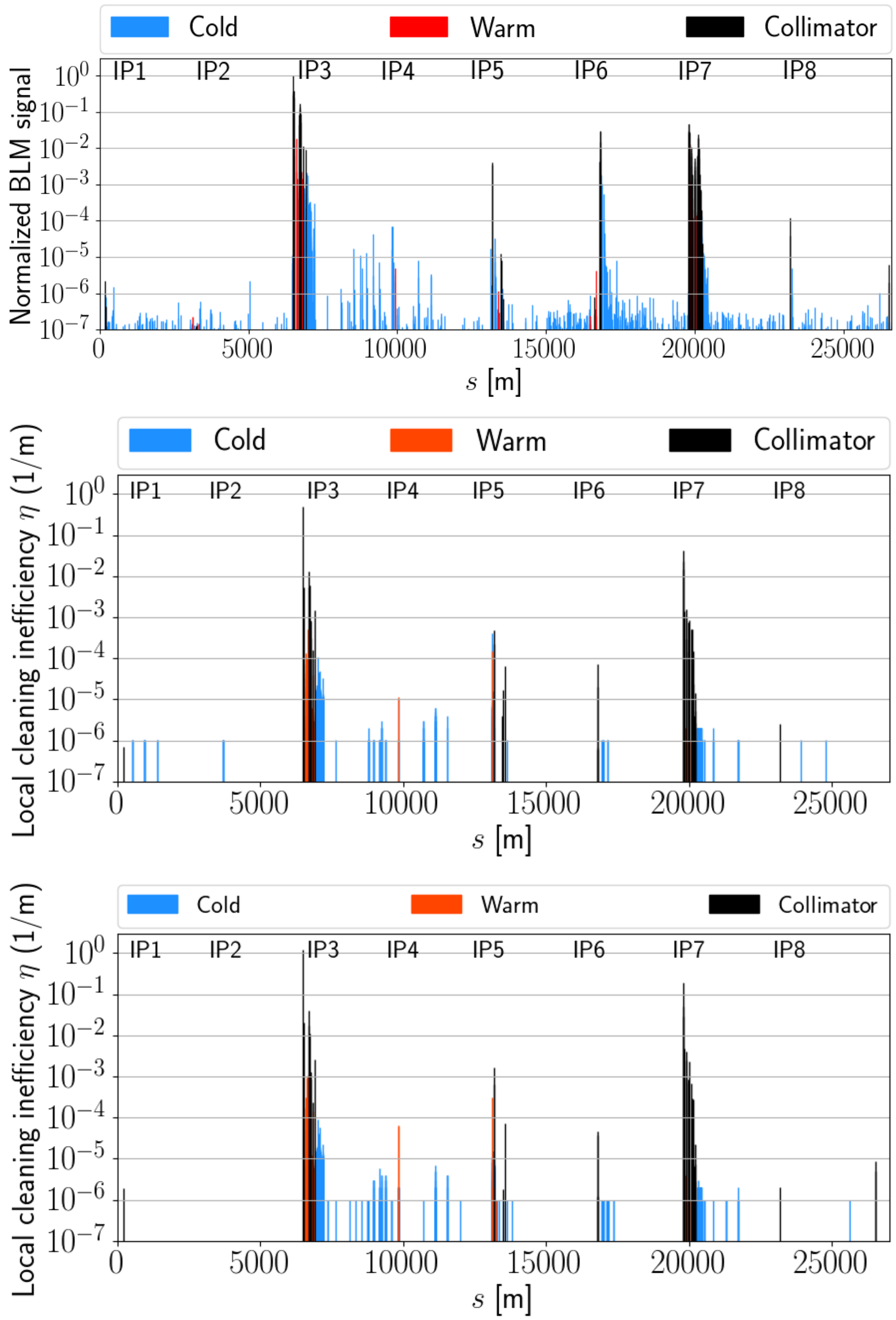

Figure 10: Comparison of the different loss maps obtained using a negative RF frequency shift (positive δ) of -500 Hz in measurement (top) and from simulation using 10^4 turns (middle) and using the simplified model with the initial distribution sampled at the collimator location for a positive dp/p (bottom).

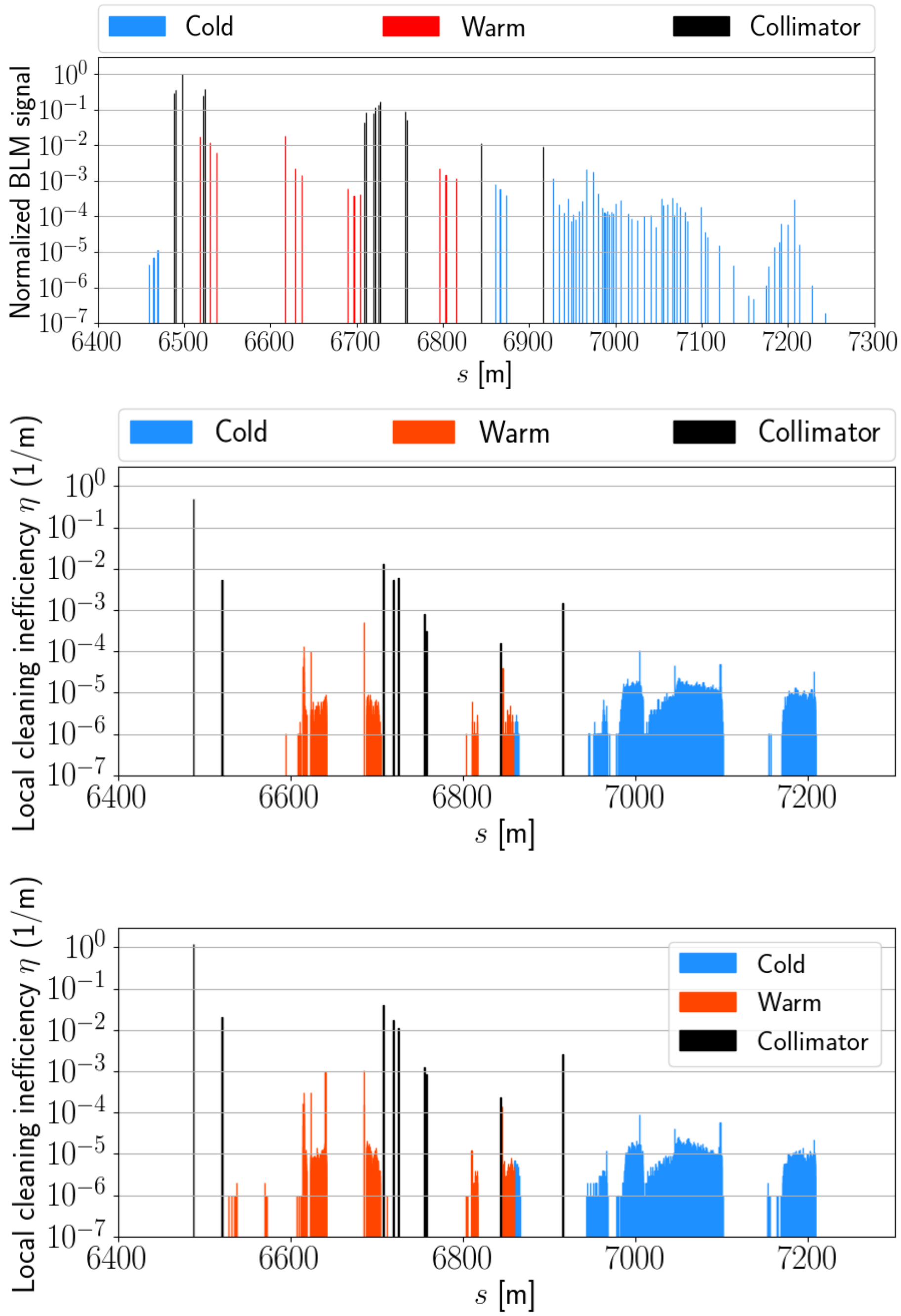

Figure 11: Zoom in IR3 of the different loss maps obtained using a negative RF frequency shift (positive dp/p) of -500 Hz in measurement (top) and during 10^4 turns (middle) and using the simplified model with the initial distribution sampled at the collimator location for a positive dp/p (bottom).

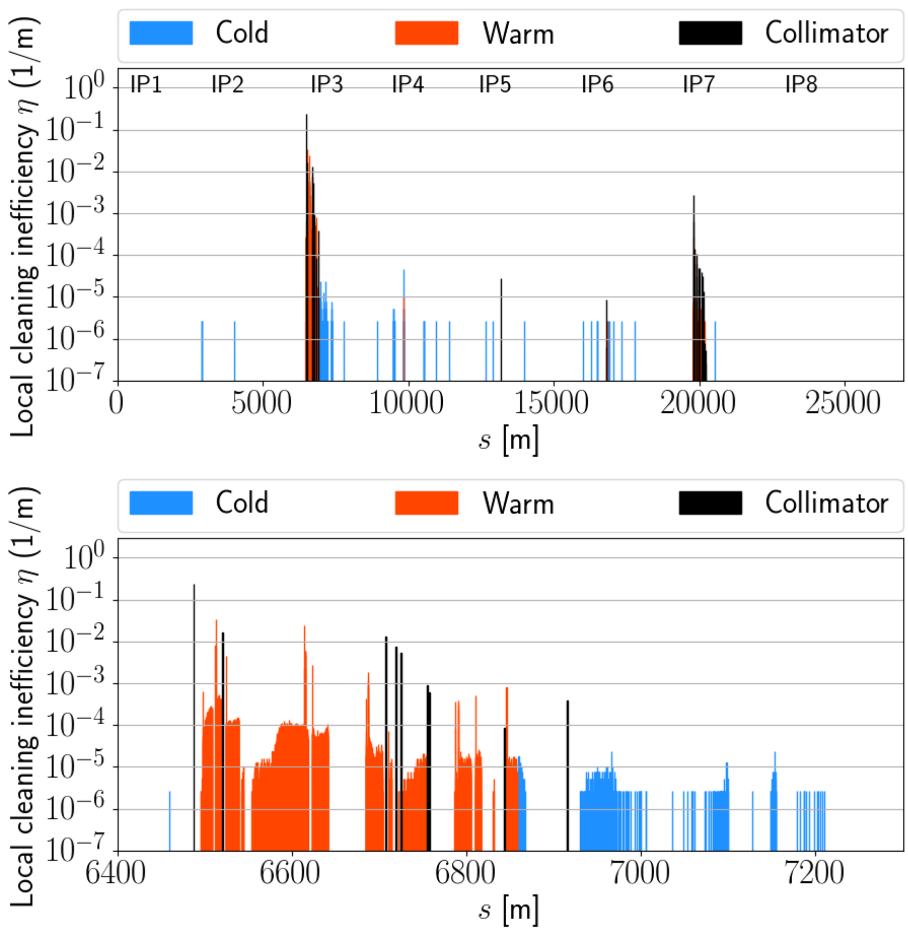

Figure 12: Off-momentum loss map simulated at the start of the ramp for the HL-LHC B1 using the full number of turns. Full ring (top) and IR3 region (bottom).

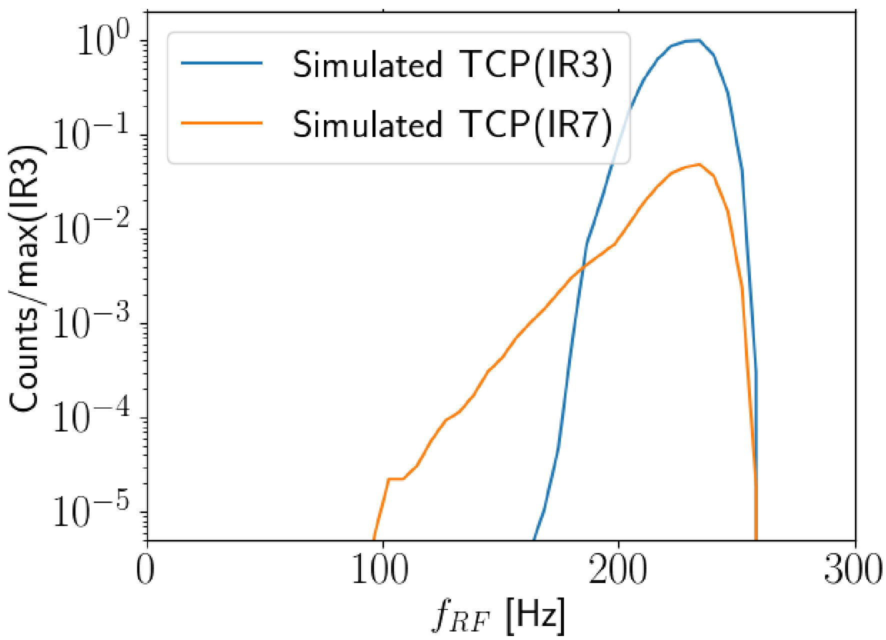

Figure 13: Evolution of the losses at the primary betatron collimator in IR7 and the primary momentum collimator in IR3 as a function of the frequency shift of -500 Hz during 10^4 turns for the HL-LHC. Losses are normalized to the peak losses in IR3

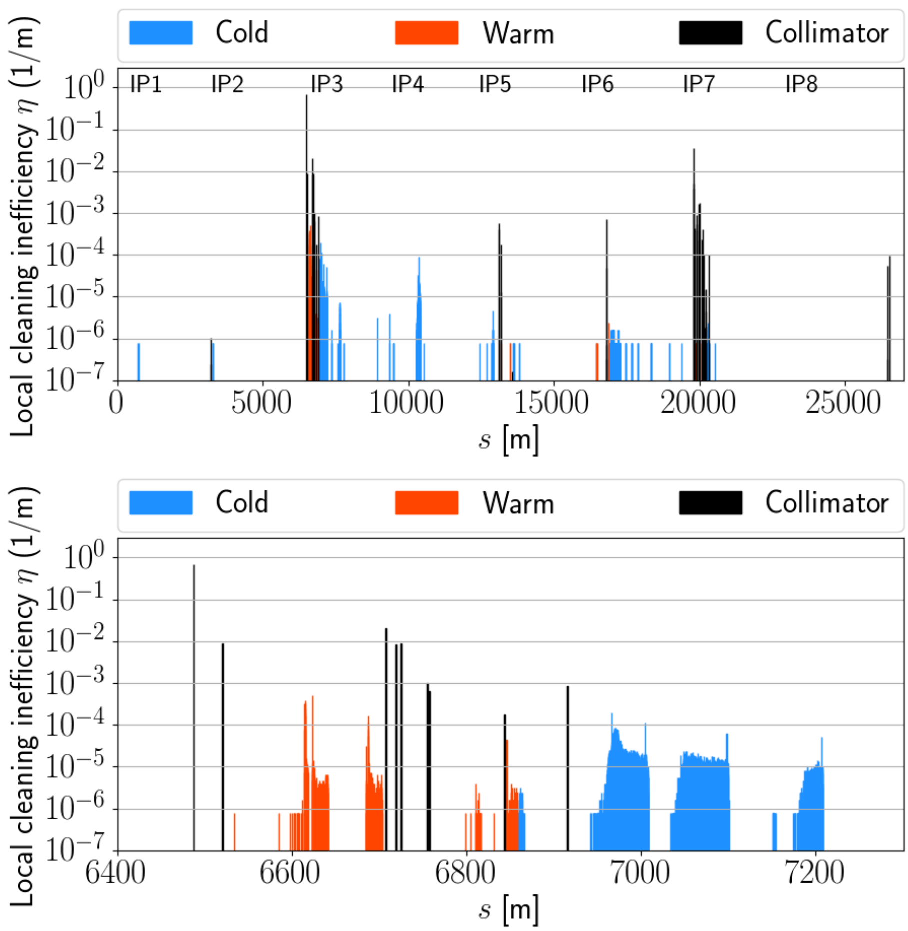

Figure 14: Off-momentum loss map simulated using the method of the RF frequency shift of -500 Hz for 10^4 turns for the HL-LHC B1. Full ring (top) and IR3 region (bottom).